A&A 635, A72 (2020)
https://doi.org/10.1051/0004-6361/201936991

Astronomy & Astrophysics

Type Ia supernovae from non-accreting progenitors

J. Antoniadis (I. Αντωνιάδης)[1,2], S. Chanlaridis (Σ. Χανλαρίδης)[2], G. Gräfener[2], and N. Langer[2,1]

[1] Max Planck Institut für Radioastronomie, Auf dem Hügel 69, 53121 Bonn, Germany
e-mail: jantoniadis@mpifr-bonn.mpg.de
[2] Argelander Institut für Astronomie, Auf dem Hügel 71, 53121 Bonn, Germany

Received 25 October 2019 / Accepted 21 January 2020

ABSTRACT

Type Ia supernovae (SNe Ia) are manifestations of stars that are deficient in hydrogen and helium, and disrupt in a thermonuclear runaway. While explosions of carbon-oxygen white dwarfs are thought to account for the majority of events, part of the observed diversity may be due to varied progenitor channels. We demonstrate that helium stars with masses between ∼1.8 and 2.5 $M_\odot$ may evolve into highly degenerate cores with near-Chandrasekhar mass and helium-free envelopes that subsequently ignite carbon and oxygen explosively at densities of $\sim(1.8\text{–}5.9)\times10^9$ g cm^{-3}. This occurs either due to core growth from shell burning (when the core has a hybrid CO/NeO composition), or following ignition of residual carbon triggered by exothermic electron captures on ^{24}Mg (for a NeOMg-dominated composition). We argue that the resulting thermonuclear runaway is likely to prevent core collapse, leading to the complete disruption of the star. The available nuclear energy at the onset of explosive oxygen burning suffices to create ejecta with a kinetic energy of $\sim10^{51}$ erg, as in typical SNe Ia. Conversely, if these runaways result in partial disruptions, the corresponding transients would resemble SN Iax events similar to SN 2002cx. If helium stars in this mass range indeed explode as SNe Ia, then the frequency of events would be comparable to the observed SN Ib/c rates, thereby sufficing to account for the majority of SNe Ia in star-forming galaxies.

Key words. binaries: general – stars: evolution – supernovae: general

1. Introduction

Despite their central role in Astrophysics and Cosmology, the origin and physics of Type Ia supernovae (SNe Ia) remain uncertain (Maoz et al. 2014). Typical SN Ia luminosities ($\sim10^{43}$ erg s^{-1}) and ejecta velocities ($\sim10^4$ km s^{-1}) require ^{56}Ni masses and kinetic energies of $\sim0.6\,M_\odot$ and $\sim10^{51}$ erg. These properties suggest that SNe Ia are most likely stars that disrupt in thermonuclear explosions, rather than core-collapse events. Carbon-oxygen white dwarfs (CO WDs) approaching the Chandrasekhar-mass limit ($M_{\rm Ch}$) are the most promising progenitor systems because they can produce explosions that are broadly consistent with observations (Nomoto 1982; Wang & Han 2012; Churazov et al. 2014).

Conventional stellar evolution channels produce stable CO WDs with masses below ∼1.1 $M_\odot$. Consequently, matter accretion onto the WD is required to trigger an explosion, either through stable transfer from a donor star (single-degenerate channels; SD), or in a merger event (double-degenerate and core-degenerate channels; DD and CD). Thus far, all of the binary models encounter substantial difficulties in providing a self-consistent model for SNe Ia (Livio & Mazzali 2018; Soker 2019). For instance, SD channels require considerable fine-tuning of the mass accretion rate for the WD to grow in mass. In addition, the interaction between the SN blast and the donor star or the circumbinary material is expected to produce signatures that are rarely or never seen, for example, some contribution to the SN luminosity at early times (Kasen 2010), radio synchrotron emission (Harris et al. 2016), and Hα emission due to unburned hydrogen. DD mergers, on the other hand, may produce a variety of outcomes, ranging from prompt explosions to long-lived remnants or the delayed formation of a neutron star (Livio & Mazzali 2018). In addition, their overall contribution to the observed SN Ia rate may be too low (van Kerkwijk et al. 2010; Claeys et al. 2014; Sato et al. 2015).

Over the past 50 years, systematic studies of SN Ia explosions have revealed a large diversity in their properties (Taubenberger 2017). Notable outliers include luminous (e.g. SN 1991T; Filippenko et al. 1992) and ultra-luminous (e.g. SNLS-03D3bb; Howell et al. 2006) SNe; SN 1991bg-like transients that are faint and evolve fast (Ruiz-Lapuente et al. 1993); peculiar SN 2002cx-like SNe, also known as SNe Iax, that may be pure thermonuclear deflagrations of helium-deficient compact objects (e.g. Li et al. 2003; Branch et al. 2004; Magee et al. 2016, 2019; Jha 2017); and SN 2012ca-like events, dubbed SNe Ia-CSM, for which there is evidence of interaction with a dense circum-stellar medium (Bochenek et al. 2018). Even among "normal" SNe Ia the scatter in rise times, maximum luminosities, ejecta velocities, and spectral evolution is appreciable (Livio & Mazzali 2018). Finally, there seems to be a correlation with environment, as star-forming galaxies typically host more and brighter SNe Ia (Maoz et al. 2014).

While part of this diversity can be understood within the framework of SD and DD/CD families, additional evolutionary pathways may exist that lead to SNe Ia. For instance, it has long been known that intermediate-mass stars form degenerate cores after helium burning. These may ignite carbon explosively if the core mass is allowed to grow as a result of shell burning (Rose 1969; Arnett 1969; Wheeler 1978). This scenario became unlikely when it was made clear that the loss of the hydrogen envelope during the AGB evolution ends the core growth rather early, which can only potentially be prevented in the most massive AGB stars (see Iben & Renzini 1983, and references therein). In this case, however, the emerging supernova would be a H- and He-rich SNe 1.5. Waldman & Barkat (2006) and Waldman et al. (2008) have considered the possible connection

between ONe cores and SNe Ia in more detail, demonstrating that some helium stars with (C)NeO cores can explode before any significant deleptonization due to electron captures on ^{20}Ne occurs. Their models still retain a small He-rich envelope at the end, and therefore, it is again unclear if such transients would appear as classical SNe Ia.

In spite of these works, ONe cores are generally thought to produce massive WDs or core-collapse electron-capture supernovae (ECSNe; e.g., Nomoto & Kondo 1991; Gutierrez et al. 1996; Takahashi et al. 2013). However, recent three-dimensional hydrodynamical simulations of oxygen deflagrations in ONe cores at central densities $\geq 10^{10}$ g cm^{-3}, that is, after the onset of electron-captures on ^{20}Ne, suggest that a large fraction of the star ($\geq 1\,M_{\odot}$) may be ejected in a so-called thermonuclear ECSN, leaving behind only a small bound remnant (Jones et al. 2016, 2019).

In light of these results, we revisit the work of Waldman & Barkat (2006) and Waldman et al. (2008) using modern tools and updated input physics. We demonstrate that a thermonuclear runaway leading to a SN Ia can indeed be initiated during the late evolution of a degenerate core of neon-oxygen (NeO) or carbon-neon-oxygen (CNeO) composition as it approaches $M_{\rm Ch}$. We show that near-$M_{\rm Ch}$ (C)NeO cores originating from intermediate-mass helium stars ($\sim$1.8–2.5 $M_{\odot}$), a common product of binary interactions, can ignite their residual carbon and oxygen explosively at densities $\lesssim 6\times10^{9}$ g cm^{-3}, before the onset of ^{20}Ne(e^{-},$\nu_{\rm e}$)^{20}F electron-capture reactions at $\sim 10^{10}$ g cm^{-3} (Sect. 2). In addition, during the final evolutionary stages, the envelope inflates significantly and is lost promptly through winds or binary interaction. Consequently, the star is helium free when it is brought to thermonuclear explosion. The available nuclear energy at the time of central oxygen ignition suffices to unbind the star and to yield ejecta with kinetic energies comparable to what is expected for classical SNe Ia (Sect. 2.5). This mechanism does not require accretion from the binary companion and therefore may contribute significantly to the SN Ia rate in young stellar populations (Sect. 3).

2. (C)NeO cores: formation and evolution

2.1. Overview

Degenerate stellar cores of NeO composition form inside stars with zero-age main-sequence (ZAMS) masses between $\sim$7 and 11 $M_{\odot}$ (e.g. Poelarends 2007; Poelarends et al. 2008; Farmer et al. 2015). After core helium burning, such stars enter a super-asymptotic giant branch (SAGB) phase, characterized by a dense CO core and an extended hydrogen envelope. As the core becomes increasingly more degenerate, it cools substantially through thermal neutrino emission. An important consequence is that the critical temperature for ^{12}C ignition is first attained off-center, creating a turbulent flame that propagates inwards (Siess 2006).

Carbon burning in SAGB stars may be affected by complex mixing processes due to a combination of inverse composition gradients, overshooting, semi-convection, and rotation. The penetration of Ne/O/Na/Mg ashes into unburned regions may significantly affect the propagation of the burning front. Mixing generally reduces the rate of thermonuclear reactions, leaving behind a substantial amount of residual carbon. In extreme cases, the flame can be quenched completely, resulting in a hybrid structure with a CO core that is surrounded by a NeO mantle (Denissenkov et al. 2013).

The subsequent evolution and final fate of these stars depends critically on the competition between neutrino cooling due to the presence of ^{23}Na ^{23}Ne and ^{25}Mg ^{25}Na Urca pairs and compressional heating due to core growth from the helium-burning shell (Schwab et al. 2017). SAGB stars are subject to significant dredge-up and thermally unstable shell burning. This may substantially affect the ability of the core to grow fast enough in mass.

However, thermal pulses and dredge-up episodes do not occur when the hydrogen envelope is lost, for example, through strong winds or interactions in a multiple system (Poelarends 2007; Poelarends et al. 2008; Woosley 2019). In this case, helium shell burning is stable, allowing the core to approach the Chandrasekhar-mass limit. We build detailed numerical models below to investigate the combined effects of residual unburned ^{12}C, Urca cooling, and constant mass growth from shell burning in the late evolution of (C)NeO cores that originate from helium stars.

2.2. Numerical calculations: input physics

We used the code MESA (version 10386) to follow the evolution of two helium-star models, M1 and M2, with masses of 2.5 and 1.8 $M_{\odot}$, respectively. The initial models have uniform compositions with $Y = 0.98$ and $Z = 0.02$ (solar abundances are taken from Grevesse & Sauval 1998). We employed a nuclear network that considers 43 isotopes, from ^{1}H to ^{58}Ni. Reaction rates were based on the `JINA reaclib v2.0` compilation (Cyburt et al. 2010). Electron screening factors and cooling rates from thermal neutrinos were evaluated as in Farmer et al. (2015), and references therein. Weak interaction rates were taken from Suzuki et al. (2016). Wind mass-loss rates were calculated using the MESA `Dutch` compilation of recipes (Paxton et al. 2013), which is independent of composition. We used Type 2 opacities during and after core helium burning.

Our baseline model considers convection, thermohaline, and semi-convectional mixing. Convective stability was evaluated using the Ledoux criterion. By default, MESA uses the standard mixing-length theory (MTL; Cox & Giuli 1968) for convective mixing and energy transport. However, following carbon burning, both our models develop dynamically unstable super-Eddington envelopes, causing numerical difficulties. For this reason, we decided to employ the "enhanced" MLT option available in MESA (Paxton et al. 2013), which artificially reduces the super-adiabatic gradient, leading to a higher convective energy transport efficiency. This allowed us to follow the evolution of the core after carbon burning without interruptions. We further discuss this choice and its effect on the envelope evolution and the final mass in Sect. 4. The MLT mixing length parameter was set to $\alpha_{\rm MLT} = 2.0$ for both models. For thermohaline mixing we employed the Kippenhahn et al. (1980) treatment, setting $D_{\rm TH} = 1.0$ for the diffusion coefficient. Semi-convection was evaluated following Langer et al. (1983), adopting an efficiency parameter of $\alpha_{\rm SEM} = 1.0$. Our models do not employ the predictive convective boundary mixing approach described in Paxton et al. (2018).

While M1 does not consider the effects of convective overshoot ($f_{\rm ov} = 0.0$), in M2, we set $f_{\rm ov} = 0.014$ across all convective boundaries, including the base of the carbon-burning flame. While mixing at this interface is unlikely (Lecoanet et al. 2016), we used this as a means to quench the flame before it reached the center. Other processes such as rotation and thermohaline mixing can lead to the same outcome for similar initial helium core masses (Farmer et al. 2015). The MESA inlists are publicly available[1]. An extended grid exploring a broad range of

[1] https://zenodo.org/record/3580243#.XfjNjpNKjUI

initial masses, metallicities, overshooting, and wind parameters will be presented in an accompanying paper (Chanlaridis et al., in prep.).

2.3. Simulation results

Figure 1 shows Kippenhahn diagrams for M1 and M2, focusing on the evolution after central helium depletion. M1 first ignites carbon at mass coordinate ∼0.3 $M_\odot$, when the total mass is 2.25 $M_\odot$, and the CO core has a mass of ∼1.15 $M_\odot$. The initial flame is followed by secondary flashes propagating in both directions. Some of these episodes seem to occur only after a small critical mass of carbon has been accumulated below the burning shell. The entire carbon-burning phase lasts for about 40 000 yr. During most of this time, the star is a red giant with a low-density convective envelope ($R \simeq 125\,R_\odot$, $\log_{10}(T_{\rm eff}/{\rm K}) \simeq 3.75$, and $\log_{10}(L/L_\odot) \simeq 4.3$), and loses mass at a rate of $\dot{M} \simeq 10^{-6}\,M_\odot\,{\rm yr}^{-1}$, in good agreement with the recent *Kepler* models (Woosley 2019). These models employ the mass-loss scheme of Yoon (2017), which is more specifically targeted to helium stars. While the mass-loss strength is highly uncertain, it has recently been suggested that the winds during the helium and carbon burning phases in low-mass helium stars may be less powerful than the `Dutch` schemes predict because no Wolf-Rayet stars are seen in this mass range (Gräfener et al. 2017; Vink 2017). In this case, the cores in our models could grow faster.

As the core contracts and its surface gravity increases, the surrounding burning shells become progressively thinner. The envelope responds by expanding, and the stellar structure closely resembles that of an SAGB core. Interestingly, Woosley (2019) found that only helium stars with masses between ∼1.6 and 3.2 $M_\odot$ develop sufficiently thin helium-burning shells to cause envelope inflation. This means that higher mass stars would likely retain a significant fraction of the outer layer until the end, leading to Type Ib SN explosions.

The last ∼5000 yr of the evolution are characterized by vigorous burning in two neighbouring shells that eventually merge, resulting in violent burning, at $t \simeq 2.41$ Myr (Fig. 1). In this phase, the star reaches extremely high luminosities of up to $\log L/L_\odot = 6.25$, generating a strong stellar wind that lasts for ∼3000 yr and eventually removes the remaining He-rich envelope. The evolution of the envelope during this stage critically depends on the energy transport mechanism above Eddington lumonisities. With the enhanced MLT option employed in our calculations, M1 briefly becomes a yellow supergiant as the envelope expands to $R \simeq 900\,R_\odot$ while remaining dynamically stable. The resulting strong wind of $\dot{M} \simeq 10^{-3.8}\,M_\odot\,{\rm yr}^{-1}$ is in the same range as the theoretically expected maximum values for super-Eddington outflows (Owocki et al. 2004; Smith & Owocki 2006). Conversely, using standard MLT, the envelope becomes dynamically unstable and our calculations encounter numerical difficulties just as the star leaves its Hayashi track, when the core has a mass of 1.32 $M_\odot$. By extrapolating the core-growth rate, the core of the star would likely still reach $M_{\rm Ch}$. Because our helium star may be the product of close binary evolution, at this stage, further interactions would easily remove the envelope because its binding energy corresponds to only a minuscule fraction of the orbital energy reservoir.

Either way, the combination of higher mass loss from both winds and binary interaction and vigorous burning leads to the complete depletion of helium in the envelope. Following the neon flash, the small residual envelope contracts and the wind ceases completely for the last ∼5000 yr (Fig. 1). Our model stopped when the star had a mass of 1.39 $M_\odot$ (see Sect. 2.4).

The evolution of the envelope in M2 is similar (Fig. 1). Here, the star expands twice, first for ∼5000 yr ($t = 5.005$ Myr in Fig. 1) and then again briefly for some ∼500 yr ($t = 5.015$ Myr), reaching a maximum size of 300 $R_\odot$. The mass-loss rate mostly remains below $10^{-6}\,M_\odot\,{\rm yr}^{-1}$. In M2, carbon ignites near mass coordinate 1.1 $M_\odot$, just as the star begins to develop an SAGB structure. The flame is quenched after only 0.1 $M_\odot$ of material has been converted into NeO, leaving behind a hybrid CO-NeO structure. Without overshooting, the flame propagates all the way to the centre, converting the entire core into ONe (see model M2b in Fig. 1). The final mass of M2 (and M2b) is 1.37 $M_\odot$.

To summarise, during the final evolutionary stages, both models are helium depleted and nearing $M_{\rm Ch}$. The ability of the core to grow in mass depends somewhat on the uncertain mass-loss rate during the final burning phases. If the envelope is lost too early during the SAGB phase (which does not seem to be the case), then the two stars would leave behind white dwarfs with masses ≤1.38 $M_\odot$, and ONe and CO-ONe composition respectively. Conversely, if the envelope is retained for long enough, as we find in our models, then the central density increases sufficiently to trigger either electron captures on ^{24}Mg or central carbon ignition. In the following section we examine the evolution of the core during this phase.

2.4. Oxygen ignition and thermonuclear runaway

Figure 2 gives an overview of the central density and temperature evolution for models M1 and M2. Following the main carbon-burning episode, both stars continue to contract but cool as a result of neutrino emission. As shell burning intensifies, compressional heating eventually balances off neutrino losses, at $\log_{10}(\rho_{\rm c}/{\rm g\,cm^{-3}}) \simeq 8.3$ and 8.0 for M1 and M2, respectively. The subsequent evolution depends on the composition.

For M1, the degenerate core is composed mostly of neon and oxygen. The most abundant isotopes have $X(^{16}{\rm O}) \simeq 0.43$, $X(^{20}{\rm Ne}) \simeq 0.42$, $X(^{24}{\rm Mg}) \simeq 0.1$, $X(^{12}{\rm C}) \simeq 0.011$, $X(^{23}{\rm Na}) \simeq 0.037$, and $X(^{25}{\rm Mg}) \simeq 0.001$. Between $\log_{10}(\rho_{\rm c}/{\rm g\,cm^{-3}}) = 9.05$ and 9.25, the temperature drops to $\log_{10}(T_{\rm c}/{\rm K}) \simeq 8.2$ as a result of the ^{25}Mg ^{25}Na and ^{23}Na ^{23}Na direct Urca reactions. At higher densities, neutrino cooling ceases completely, and the temperature rises again (Fig. 2). When $\log_{10}(\rho_{\rm c}/{\rm g\,cm^{-3}}) = 9.65$, exothermic electron captures on ^{24}Mg and ^{24}Na start to occur at a substantial rate, raising the temperature adequately to ignite carbon. In turn, this triggers oxygen burning and a thermonuclear runaway at $\log_{10}(\rho_{\rm c}/{\rm g\,cm^{-3}}) = 9.77$. This ignition density is lower than the $\log_{10}(\rho_{\rm c}/{\rm g\,cm^{-3}}) \geq 9.97$ typically expected for oxygen deflagrations in pure NeO cores (Jones et al. 2019). As a consequence, severe deleptonization due to ^{20}Ne electron captures is likely avoided. To demonstrate the importance of residual carbon, we computed a variation of this model in which the energy contribution of all carbon-consuming reactions was artificially suppressed following the main carbon-burning phase (model M1B in Fig. 2). In this case, oxygen ignites above $\log_{10}(\rho_{\rm c}/{\rm g\,cm^{-3}}) \simeq 10$ and only after ^{20}Ne electron captures have started to occur at a significant rate. This means that in the absence of residual carbon, this star would produce a core-collapse or a thermonuclear ECSN (Jones et al. 2016).

M2 is composed mostly of carbon and oxygen, with $X(^{12}{\rm C}) = 0.38$ and $X(^{16}{\rm O}) = 0.60$, respectively. Here, ^{23}Na is not abundant enough to cause substantial cooling. Consequently, carbon, which is significantly more abundant than M1, ignites at $\log_{10}(\rho_{\rm c}/{\rm g\,cm^{-3}}) = 9.26$.

The evolution following central oxygen ignition is not adequately modelled in our 1D simulations. M2 will most likely

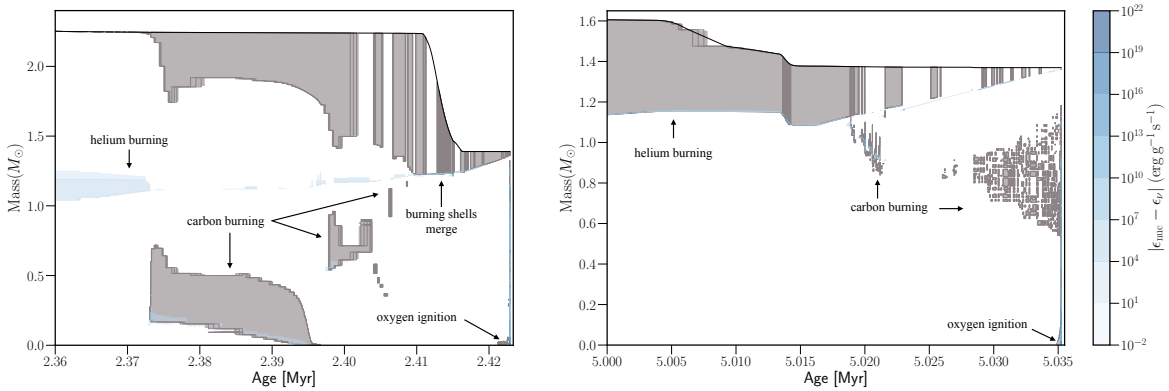

Fig. 1. Kippenhahn diagrams following the evolution of M1 (*left*) and M2 after core helium depletion. Blue shaded areas indicate regions in which nuclear burning occurs, i.e. locations for which the nuclear energy $\epsilon_{\rm nuc}$ exceeds energy losses due to neutrino emission, ϵ_ν. Grey regions are subject to convective mixing. $t = 0$ corresponds to the onset of core helium burning.

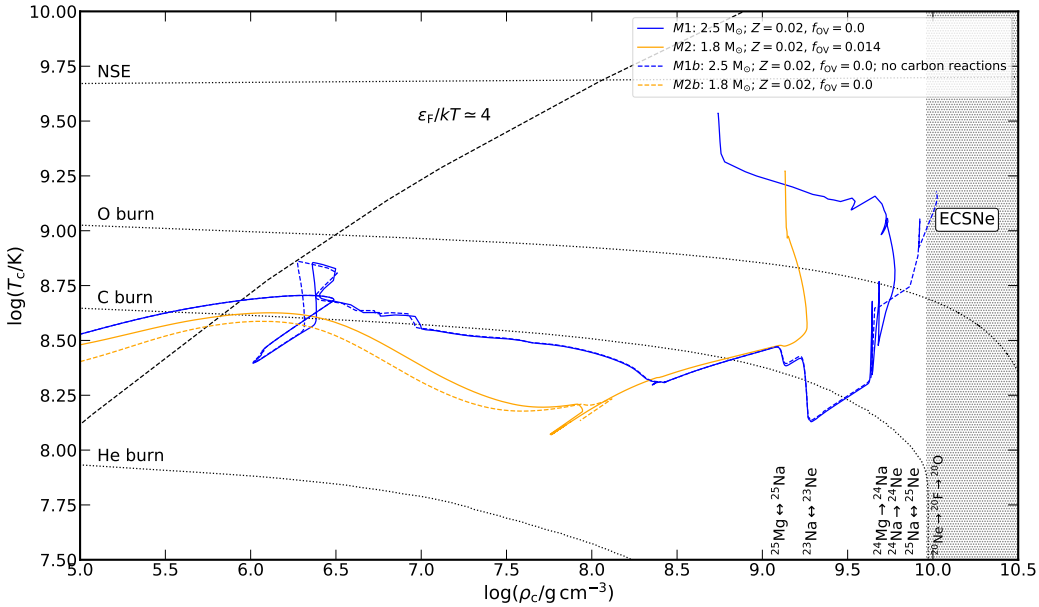

Fig. 2. Evolution of the core density and temperature for M1 and M2. The dashed line shows the approximate boundary for electron degeneracy. Burning thresholds for a 100% abundance of the corresponding species are indicated with dotted lines. The NSE threshold assumes an equilibrium timescale of 1 s. In model M1b, the energy contribution of carbon-consuming reactions is set to zero (see text). M2b shows the core evolution of a 1.8 $M_\odot$ without overshooting. While this model stopped at $\log_{10}(\rho_c/{\rm g\,cm^{-3}}) \simeq 8.2$ because of numerical convergence issues, the final core mass is similar to M2.

disrupt in a SN Ia, as the composition and ignition conditions resemble closely those found in standard CO WD SN Ia progenitors (Nomoto 1982). While the fate of M1 is less certain, a thermonuclear explosion is also the most likely outcome: firstly, the available nuclear energy is sufficient to unbind the star (see below). Secondly, the ignition density is only slightly higher than what is typically considered for CO WD SN Ia progenitors. The deflagration ashes will therefore likely be buoyant, leading to expansion, which in turn will limit the deleptonization rate. This hypothesis is strongly supported by 3D hydrodynamic simulations of ECSN deflagrations by Jones et al. (2016, 2019): their least compact progenitor ingites at $\log_{10}(\rho_c/{\rm g\,cm^{-3}}) = 9.90$ but still manages to eject $\sim 1\,M_\odot$ of material. Similarly, Marquardt et al. (2015) simulated ONe WD detonations at lower densities and demonstrated that the explosion is practically identical to a typical SN Ia. Interestingly, in our 1D simulations, both models experience significant expansion. This is most likely the result of (over-)efficient convection, which also homogenizes the inner $\sim 1\,M_\odot$ of the core.

2.5. Energetics and nucleosynthesis

Figure 3 shows the density profiles of M1 and M2 at maximum compactness ($\log_{10}(\rho_c/{\rm g\,cm^{-3}}) = 9.77$ and 9.22, respectively) and at the end of our simulations. At the onset of oxygen ignition, M1 and M2 have binding energies of $E_{\rm bind} = -5.76 \times 10^{50}$ and -5.16×10^{50} erg and average electron fractions of $Y_e = 0.496$ and 0.499, respectively. If these progenitors were to produce a SN Ia of typical composition, with $\sim 0.7\,M_\odot$ of nickel and iron and $0.6\,M_\odot$ of Si-group elements, the corresponding kinetic energies of the ejecta would be $E_{\rm kin} = E_{\rm nuc} - E_{\rm bind} \simeq 0.83 \times 10^{51}$ and 1.17×10^{51} erg. Obviously, the nucleosynthesis yields depend on the actual Y_e and density profiles during explosive burning. If M1 achieves nuclear statistical equilibrium (NSE) before any significant expansion and deleptonization, then it would produce mostly stable iron-peak elements and $\sim 0.3\,M_\odot$ of ^{56}Ni, resulting in a sub-luminous explosion that would resemble a SN Iax. Similarly, low nickel masses would be expected if the deflagration wave never transitions to a detonation. On the other hand,

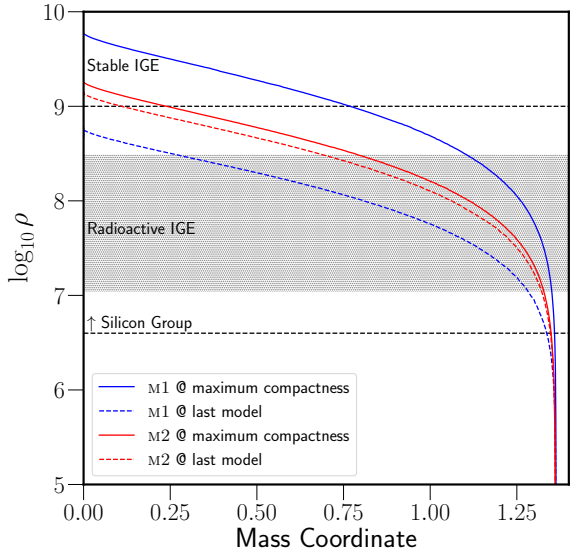

Fig. 3. Density profiles at maximum compactness (solid lines) and at the end of our MESA calculations (dashed lines). Regions indicating approximate burning regimes as in Seitenzahl & Townsley (2017).

if NSE is achieved at densities similar to our last MESA model, following an initial expansion (Fig. 3), more than 1 $M_\odot$ of ^{56}Ni can be produced, with only moderate amounts of iron. Similarly, M2 could produce up to 1.3 $M_\odot$ of iron elements if it does not expand any further.

3. Rates and delay times

An additional proxy for the potential connection between exploding (C)NeO cores and SNe Ia is a comparison between their occurrence rates. A zeroth-order upper bound on the number of stripped near-Chandrasekhar mass (C)NeO cores per unit solar mass of star formation, $n_\star$, is simply the number of stars, $n_{\rm He1.8-2.5}$, that develop helium cores in the relevant mass range, here taken to be $1.8 \lesssim M_{\rm He}/M_\odot \lesssim 2.5$, based on our simulations and the recent results of Woosley (2019) and Farmer et al. (2015), who also found that carbon ignites off-center in this mass range, independently of convective overshoot assumptions.

Based on Farmer et al. (2015), such helium stars originate from ZAMS stars with masses $\sim 7 \ldots 11\,M_\odot$. Adopting a Chabrier (2005) initial mass function (IMF) for the aforementioned mass range, we find $n_\star = n_{\rm He1.8-2.5} \simeq 0.0059$, which is larger than the observed number of SNe Ia per solar mass, $n_{\rm SN\,Ia} \simeq 0.001-0.003$ (e.g. Claeys et al. 2014; Maoz et al. 2014). Here, we recall that the mass width for off-centre carbon burning is subject to several physical uncertainties related to winds as well as mixing and flame propagation during the carbon burning phase, for example (Sect. 2). In addition, for isolated H-rich SAGB stars, the second dredge-up also limits the mass range for which the helium core mass remains near $M_{\rm Ch}$ to about $\sim 0.1\,M_\odot$ around a ZAMS mass of 11 $M_\odot$ (cf. Fig. 1 in Podsiadlowski et al. 2004). More realistically, a maximum single-star contribution $\sim$10 times smaller than the rate estimated above would therefore be expected. However, stars in interacting multiple systems, which loose their H-rich envelopes early, avoid dredge-up. This means that most interacting stars capable of igniting carbon off-centre will also reach near-$M_{\rm Ch}$ final core masses (Podsiadlowski et al. 2004; Poelarends 2007; Poelarends et al. 2008, 2017; Chen et al. 2014; Meng & Podsiadlowski 2014; Doherty et al. 2015, and references therein).

If this channel is indeed mostly relevant to stars in multiple systems, that is, if the hydrogen envelope can only be removed through binary interactions, then only the fraction of $n_{\rm He1.8-2.5}$ in interacting binaries is relevant. Adopting the same assumptions for the initial mass range as above, $f_{\rm bin} = 0.7$ for the fraction of stars in interacting binaries (Sana et al. 2012), a Chabrier (2005) IMF for the primaries (i.e. the initially more massive stars), and a mass-ratio distribution scaling as $\propto q^{-0.1}$ (Sana et al. 2012), we find $n_\star \simeq 0.0038$. Here, systems for which both stars have initial masses between 7 and 11 $M_\odot$ are only counted once because the secondary would evolve in isolation after the primary explodes. Owing to the shape of the IMF, about 80% of the stars that contribute to the former estimate are primaries, that is, they would explode while still having a less-evolved companion.

More realistically, a significant number of these binaries would likely interact before the carbon-burning phase, thereby affecting the growth of the core and consequently the event rate. While detailed calculations are required to probe the influence of binary interactions, an upper limit on the expected rate can be obtained by comparing the frequency of progenitor systems relative to the SN Ib/c progenitors, assuming that the latter are dominated by stripped helium stars with masses $\geq 2.5\,M_\odot$ (Woosley 2019), which evolve similarly. Adopting the same IMF and initial mass range as above, we find a total rate of $\sim 0.8-1.0$ times the SN Ib/c rate, which is consistent with observations (Branch & Wheeler 2017, and references therein).

In addition to the total number of SNe Ia, a property that may be more challenging to match with observations is the evolution of the SN Ia rate with cosmic time. SNe Ia from such a channel would have delay times that are dominated by the main-sequence lifetime of the progenitors, that is, of order 30 to 78 Myr, for stars with ZAMS masses between 7 and 11 $M_\odot$. Binaries interacting through early Case A Roche-lobe overflow (RLO) prior to the removal of the hydrogen envelope could contribute events up to $\sim$300 Myr following star formation (corresponding to the main-sequence lifetime of a 3.5 $M_\odot$ star). These delay times could help account for the high SN Ia rates in star-forming galaxies, compared to ellipticals (Maoz & Badenes 2010; Claeys et al. 2014), but some variant of the DD channel, or more generally, a model with a delay time much longer than the main-sequence lifetime of intermediate-mass stars, would still be required to explain events with much longer delay times. However, if the (C)NeO core of a WD were to evolve in a similar way through mass accretion from a companion as in the SD scenarios, or in a merger similar to the DD and CD scenarios, then the corresponding explosion could contribute a SN Ia several Gyr after star formation (see also Kashi & Soker 2011; Chen et al. 2014; Meng & Podsiadlowski 2014; Marquardt et al. 2015; Schwab et al. 2015, 2017; Jones et al. 2016; Schwab & Rocha 2019; Kashyap et al. 2018; Augustine et al. 2019; Soker 2019, and references therein). Finally, if (C)NeO explosions produce less nickel than typical SNe Ia, then the short delay times would match those of under-luminous SNe Iax, which predominately occur in star-forming regions (Lyman et al. 2013; Jha 2017).

4. Summary

We have shown that at least some stars capable of developing near-$M_{\rm Ch}$ (C)NeO cores after losing their hydrogen envelopes may explode as SNe Ia instead of undergoing a core-collapse ECSN. For NeO compositions, the runaway seems to be triggered by the ignition of residual carbon following electron captures on ^{24}Mg, which in turn leads to explosive oxygen burning at densities below 5.9×10^9 g cm^{-3} (Sect. 2). For hybrid CO/NeO

cores, ignition is triggered by core compression at a density of 1.8×10^9 g cm^{-3}, similar to what is expected for CO WD deflagrations. For either case, the conditions at the onset of oxygen burning are such that the energetics could closely resemble a typical SN Ia or an under-luminous Iax, depending on when and if the initial deflagration transitions into a detonation (Sect. 2.5). It would be worth considering whether the differences in initial density and composition could lead to distinct nucleosynthetic signatures that would help distinguish these progenitors and/or contribute uniquely to the chemical evolution of the Galaxy (in analogy to Jones et al. 2019, for ECSNe).

The frequency of the corresponding progenitor systems is sufficient to account for a considerable fraction of the observed SN Ia rate. Our optimistic zeroth-order upper bounds in Sect. 3 suggest that SNe Ia from non-accreting progenitors could occur at the same rate as SNe Ib/c, assuming that the latter also result from stripped helium stars. Because the bulk of events would occur only ∼50 Myr after star formation, this channel is mostly relevant to star-forming galaxies. The shorter delay times compared to traditional SN Ia scenarios open further interesting avenues for constraining this model, for example by considering the abundance rations of alpha elements relative to iron in metal-poor stars.

While here we demonstrated that the helium envelope is likely lost only after the core has grown to $M_{\rm Ch}$, its evolution remains a major uncertainty for this progenitor channel. If helium is removed sufficiently early, for example as a result of binary interactions, then sub-$M_{\rm Ch}$ (C)NeO WDs would be formed instead.

In spite of the mass-loss uncertainties, if viable, this channel would help explain some of the observed SN Ia diversity. Because either star in a binary system may potentially explode as a SN Ia without accreting from its companion, the resulting events can resemble setups that are expected in all SD and DD/CD scenarios. Explosions of secondaries would follow a first core-collapse SN. This could lead to SN Ia remnants with no luminous surviving stars, high proper motions due to a kick from the first SN (like the *Kepler* SN remnant, Chiotellis et al. 2012), and possibly associated with a neutron star. Because the envelope can be removed by winds, case-BB mass transfer, or a common-envelope event, some diversity is also expected in the SN environment. This in turn would influence both the appearance of the explosion and the evolution of the SN remnant. The rates estimated in Sect. 3 are also broadly consistent with the number of SNe Ia that seem to explode inside planetary nebulae (∼20%; Tsebrenko & Soker 2015).

Acknowledgements. We thank the referee for the extremely helpful report. This research made extensive use of NASA's ADS, MESA (http://mesastar.org) (Paxton et al. 2011, 2013, 2015, 2018) and Astropy (http://www.astropy.org) (Astropy Collaboration 2018). Figure 1 was created with NuGridPy (https://github.com/NuGrid/NuGridPy).

References

Arnett, W. D. 1969, ApJS, 5, 180
Astropy Collaboration (Price-Whelan, A. M., et al.) 2018, AJ, 156, 123
Augustine, C. N., Willcox, D. E., Brooks, J., Townsley, D. M., & Calder, A. C. 2019, ApJ, 887, 188
Bochenek, C. D., Dwarkadas, V. V., Silverman, J. M., et al. 2018, MNRAS, 473, 336
Branch, D., & Wheeler, J. C. 2017, Supernova Explosions: Astronomy and Astrophysics Library (Germany: Springer-Verlag GmbH)
Branch, D., Baron, E., Thomas, R. C., et al. 2004, PASP, 116, 903
Chabrier, G. 2005, The Initial Mass Function 50 Years Later, 327, 41
Chen, M. C., Herwig, F., Denissenkov, P. A., & Paxton, B. 2014, MNRAS, 440, 1274
Chiotellis, A., Schure, K. M., & Vink, J. 2012, A&A, 537, A139
Churazov, E., Sunyaev, R., Isern, J., et al. 2014, Nature, 512, 406
Claeys, J. S. W., Pols, O. R., Izzard, R. G., Vink, J., & Verbunt, F. W. M. 2014, A&A, 563, A83
Cox, J. P., & Giuli, R. T. 1968, Principles of Stellar Evolution and Nucleosynthesis (New York: McGraw-Hill)
Cyburt, R. H., Amthor, A. M., Ferguson, R., et al. 2010, ApJS, 189, 240
Denissenkov, P. A., Herwig, F., Truran, J. W., & Paxton, B. 2013, ApJ, 772, 37
Doherty, C. L., Gil-Pons, P., Siess, L., Lattanzio, J. C., & Lau, H. H. B. 2015, MNRAS, 446, 2599
Farmer, R., Fields, C. E., & Timmes, F. X. 2015, ApJ, 807, 184
Filippenko, A. V., Richmond, M. W., Matheson, T., et al. 1992, ApJ, 753, L5
Gräfener, G., Owocki, S. P., Grassitelli, L., & Langer, N. 2017, A&A, 608, A34
Grevesse, N., & Sauval, A. J. 1998, Space Sci. Rev., 85, 161
Gutierrez, J., Garcia-Berro, E., Iben, I., et al. 1996, ApJ, 459, 701
Harris, C. E., Nugent, P. E., & Kasen, D. N. 2016, ApJ, 823, 100
Howell, D. A., Sullivan, M., Nugent, P. E., et al. 2006, Nature, 443, 308
Iben, Jr., I., & Renzini, A. 1983, ARA&A, 21, 271
Jha, S. W. 2017, Handbook of Supernovae (Cham: Springer), 375
Jones, S., Röpke, F. K., Pakmor, R., et al. 2016, A&A, 593, A72
Jones, S., Röpke, F. K., Fryer, C., et al. 2019, A&A, 622, A74
Kasen, D. 2010, ApJ, 708, 1025
Kashi, A., & Soker, N. 2011, MNRAS, 417, 1466
Kashyap, R., Haque, T., Lorén-Aguilar, P., García-Berro, E., & Fisher, R. 2018, ApJ, 869, 140
Kippenhahn, R., Ruschenplatt, G., & Thomas, H.-C. 1980, A&A, 91, 175
Langer, N., Fricke, K. J., & Sugimoto, D. 1983, A&A, 126, 207
Lecoanet, D., Schwab, J., Quataert, E., et al. 2016, ApJ, 832, 71
Li, W., Filippenko, A. V., Chornock, R., et al. 2003, PASP, 115, 453
Livio, M., & Mazzali, P. 2018, Phys. Rep., 736, 1
Lyman, J. D., James, P. A., Perets, H. B., et al. 2013, MNRAS, 434, 527
Magee, M. R., Kotak, R., Sim, S. A., et al. 2016, A&A, 589, A89
Magee, M. R., Sim, S. A., Kotak, R., Maguire, K., & Boyle, A. 2019, A&A, 622, A102
Maoz, D., & Badenes, C. 2010, MNRAS, 407, 1314
Maoz, D., Mannucci, F., & Nelemans, G. 2014, ARA&A, 52, 107
Marquardt, K. S., Sim, S. A., Ruiter, A. J., et al. 2015, A&A, 580, A118
Meng, X., & Podsiadlowski, P. 2014, ApJ, 789, L45
Nomoto, K. 1982, ApJ, 253, 798
Nomoto, K., & Kondo, Y. 1991, ApJ, 367, L19
Owocki, S. P., Gayley, K. G., & Shaviv, N. J. 2004, ApJ, 616, 525
Paxton, B., Bildsten, L., Dotter, A., et al. 2011, ApJS, 192, 3
Paxton, B., Cantiello, M., Arras, P., et al. 2013, ApJS, 208, 4
Paxton, B., Marchant, P., Schwab, J., et al. 2015, ApJS, 220, 15
Paxton, B., Schwab, J., Bauer, E. B., et al. 2018, ApJS, 234, 34
Podsiadlowski, P., Langer, N., Poelarends, A. J. T., et al. 2004, ApJ, 612, 1044
Poelarends, A. J. T. 2007, PhD Thesis, University Utrecht
Poelarends, A. J. T., Herwig, F., Langer, N., & Heger, A. 2008, ApJ, 675, 614
Poelarends, A. J. T., Wurtz, S., Tarka, J., Cole Adams, L., & Hills, S. T. 2017, ApJ, 850, 197
Rose, W. K. 1969, ApJ, 155, 491
Ruiz-Lapuente, P., Jeffery, D. J., Challis, P. M., et al. 1993, Nature, 365, 728
Sana, H., de Mink, S. E., de Koter, A., et al. 2012, Science, 337, 444
Sato, Y., Nakasato, N., Tanikawa, A., et al. 2015, ApJ, 807, 105
Schwab, J., & Rocha, K. A. 2019, ApJ, 872, 131
Schwab, J., Quataert, E., & Bildsten, L. 2015, MNRAS, 453, 1910
Schwab, J., Bildsten, L., & Quataert, E. 2017, MNRAS, 472, 3390
Seitenzahl, I. R., & Townsley, D. M. 2017, Nucleosynthesis in Thermonuclear Supernovae (Springer), 1955
Siess, L. 2006, A&A, 448, 717
Smith, N., & Owocki, S. P. 2006, ApJ, 645, L45
Soker, N. 2019, ArXiv e-prints [arXiv:1912.01550]
Suzuki, T., Toki, H., & Nomoto, K. 2016, ApJ, 817, 163
Takahashi, K., Yoshida, T., & Umeda, H. 2013, ApJ, 771, 28
Taubenberger, S. 2017, Handbook of Supernovae (Cham: Springer), 317
Tsebrenko, D., & Soker, N. 2015, MNRAS, 447, 2568
van Kerkwijk, M. H., Chang, P., & Justham, S. 2010, ApJ, 722, L157
Vink, J. S. 2017, A&A, 607, L8
Waldman, R., & Barkat, Z. 2006, PhD Thesis
Waldman, R., Yungelson, L. R., & Barkat, Z. 2008, ASP Conf. Ser., 391, 359
Wang, B., & Han, Z. 2012, New Astron. Rev., 56, 122
Wheeler, J. C. 1978, ApJ, 225, 212
Woosley, S. E. 2019, ApJ, 878, 49
Yoon, S.-C. 2017, MNRAS, 470, 3970